

¹ PREPARED FOR SUBMISSION TO JINST

² **Directional Xenon Measurement**

³ ABSTRACT: Abstract...

⁴ KEYWORDS: Only keywords from JINST's keywords list please

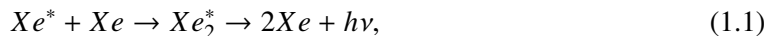
⁵ ARXIV EPRINT: [1234.56789](https://arxiv.org/abs/1234.56789)

6	Contents		
7	1	Introduction	1
8	2	Experimental Setup	2
9	2.1	Gas handling system	2
10	2.2	The Cryogenic system	4
11	2.3	The Detector	6
12	2.3.1	The Detector Chamber	6
13	2.3.2	The Sphere	6
14	3	The Data Acquisition (DAQ) System	10
15	4	Simulation	12
16	4.1	The Detector Geometry	12
17	4.2	The statistical test	12
18	5	Summary	12

19 1 Introduction

20 The use of Noble-liquid detectors in the field of astroparticle physics has increased in the past
21 decades. Detectors aiming at measuring Dark Matter (DM) particles and neutrinos properties use
22 large liquid argon or liquid xenon (LXe) chambers [1, 2]. Current and future experiment for DM
23 detectioin are tuned to detect weakly interacting massive particles (WIMPs), a postulated candiadte
24 for DM particle [3]. LXe based detectors are to date the leading in sensitivity and size for these
25 searches [4–7].

26 When a particle interacts within the LXe media, it forms a cloud of excited and ionized states
27 with typical length of 100 nm. The excited Xe (Xe^*) combines with other Xe atoms to form an
28 excited dimer state (excimer) when they decay to ground state they emit light.



29 The electrons emitted from the ionization can recombine with a surrounding atom, this process of
30 recombination provides another possibility to produce excimers,



31 Once Xe^* is produced it adds to the scintillation process explained in 1.1. There are two types of
32 Xe_2^* excimer states, singlet and triplet, with lifetime of ~ 3 ns and ~ 25 ns respectively. The wave-
33 length emitted by these states is between (175-180) nm which is lower than the lowest excitation of
34 xenon, and therefore travel through it to reach a photo-detector situated outside the LXe. Although
35 much is measured on these scintillation processes, the basic knowledge of the quantum properties
36 of these interactions is based on experiments preformed several decades ago.

37 The phenomenon of superradiance in which identical quantum states "communicate" through
38 electromagnetic field if in close proximity, is well studied. In certain conditions the emission of
39 photons from these correlated states is very different than the sum of random states. This difference
40 is in spectral, temporal and spatial properties [8, 9]. Early studies show that scintillation in LXe can
41 produce coherent amplification of light [10, 11]. These studies were focusing on the macroscopic
42 ionization using high energy density electron beams.

43 The understanding and quantification of the microscopic effects of non linear phenomena such
44 as superradiance in Lxe for a single interaction, can improve DM experiments to reduce back-
45 ground by the extra knowledge of directionality. irreducible background such as coherent neutrino
46 nucleus scattering of neutrinos from the sun can be discard.

47 In this paper we present an experimental set-up called DIREXENO (Directional Xenon) aim-
48 ing at measuring the spatial distribution of LXe scintillation light, and quantify non-isotropic emis-
49 sion.

50 2 Experimental Setup

51 The experimental setup that is described in this section, is designed to measure, the spatial and
52 temporal properties of LXe scintillation. However it is designed in a modular way, so it can serve
53 different requirements from different future experiments.

54 There are four main building blocks constructing the full setup, a schematics of them with
55 the interfaces connecting them is shown in Fig. 1. The gas handling system, which, in normal
56 working mode, drives the xenon from the detector trough a purifier and back into the detector.
57 The cryogenic system, which liquefies the xenon and delivers it to the detector part. The detector
58 system, mainly an HPFS sphere with a small bubble of LXe inside it surrounded with PMTs. Finally
59 the data acquisition (DAQ) system that supplies HV and reads the data from all sensors (e.g., PMTs,
60 pressure gauge etc.). Each building block can be replaced without effecting the others.

61 The full assembly (Fig. 2) is held on three separate racks, one for the DAQ, while the two
62 others hold the cryogenic detector and gas handling system are joined using a 100mm bar with
63 shock absorbers on both sides. Some of the guidelines for the design of DIREXENO are based
64 on [12]

65 2.1 Gas handling system

66 A typical LXe detector must keep a high level of purity. Careful selection and meticulously clean-
67 ing of all parts before mounting, is needed, however is not sufficient. The desired level of most
68 detectors of impurity concentration is at the level of 1 ppb O_2 equivalent [1]. This is crucial to
69 allow ionization electrons drift for several cm. To reach that level in a reasonable amount of time

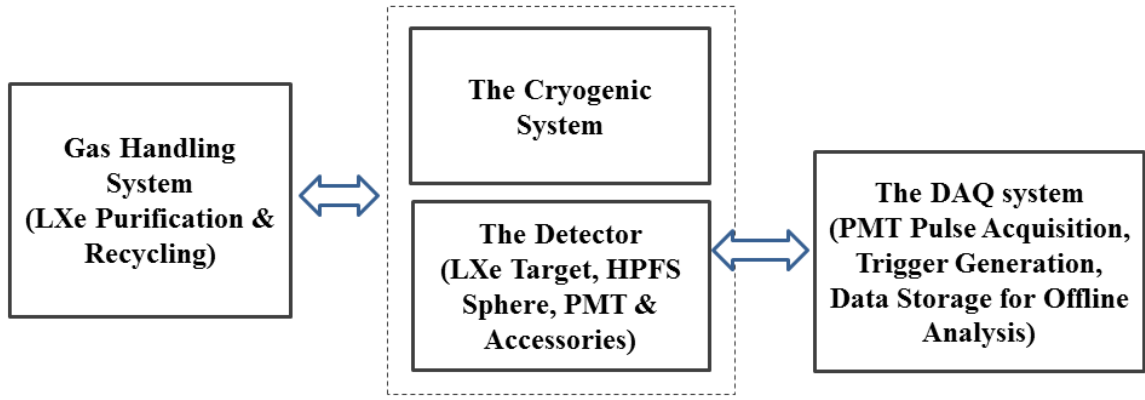


Figure 1. DIREXENO. On the left the purification system, in the middle the cryogenic and detector chamber, and on the right the Data acquisition system.

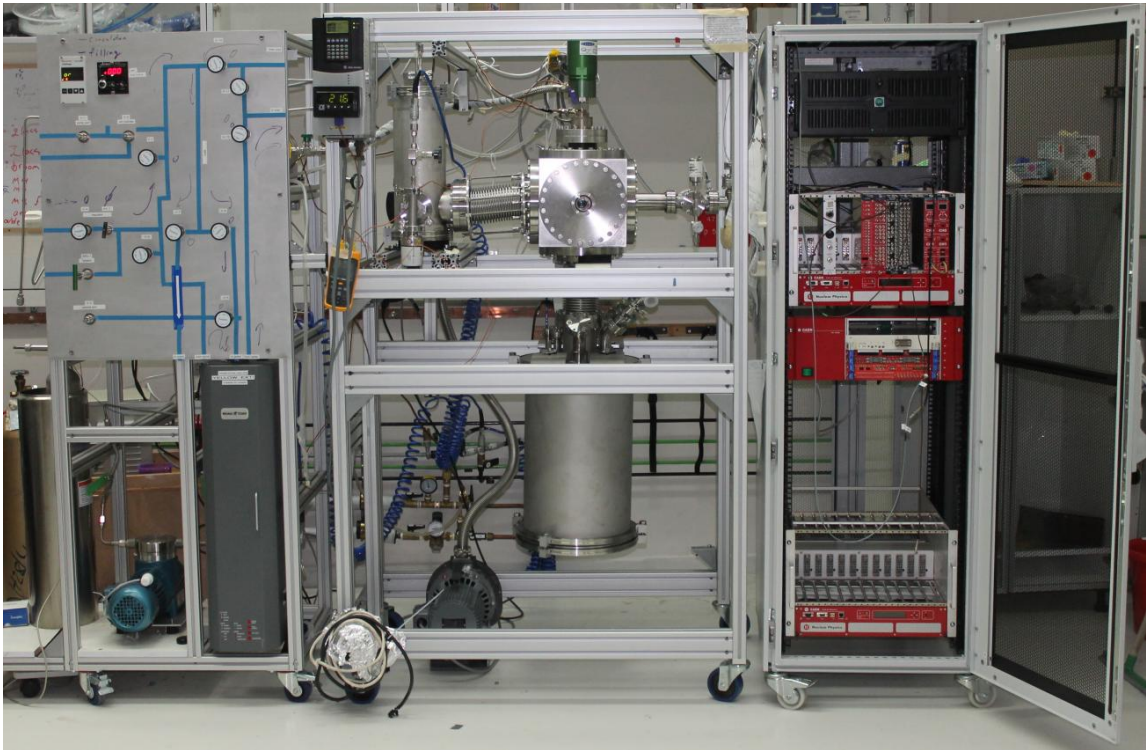


Figure 2. DIREXENO. On the left the purification system, in the middle the cryogenic and detector chamber, and on the right the Data acquisition system.

70 (several days instead of months), continuous purification is needed. The gas handling system,
71 provides this process, alongside with all gas handling operations such as filling and recuperation.

72 During purification mode, xenon is taken from the chamber (in liquid phase) passes through a
73 heat exchanger¹ where it is heated and vaporized. The xenon is forced by a KNF diaphragm pump

¹GEA GBS100M-24 plate heat exchanger

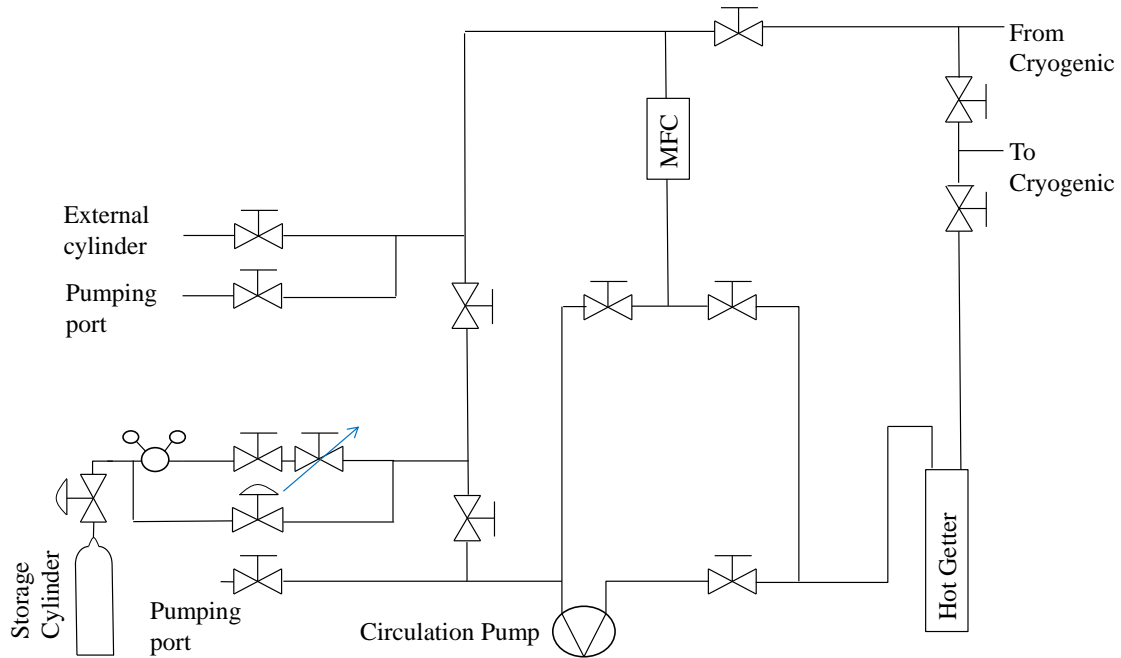


Figure 3. Schematics of the purification system. High pressure valves are indicated as valves with arcs. Needle valves are indicated as a valve with an arrow.

74 into a hot getter¹ which cleans the xenon from most impurities. The xenon also passes through an
 75 MKS Mass Flow Controller² (MFC), this allows monitoring and controlling the amount of xenon
 76 in the system.

77 After the xenon is purified, it is delivered back to the cryogenic system through the heat ex-
 78 changer, there the remained xenon gas is liquefied before it continuous back to the chamber. A
 79 schematic of this system is shown in fig. 3.

80 2.2 The Cryogenic system

81 Remote cooling is generally used in DM experiments due to background radiating from the cooler
 82 to the detector. Although in our system this is not of great importance there are still several ad-
 83 vantages to remote cooling such as: lowering acoustic noise from the cryo-cooler and flexibility to
 84 design changes. The cryogenic system is connected on one side to the gas system and on the other
 85 to the detector chamber, any change in the system (e.g, cooler type or model) requires the change
 86 of that specific part without changing the detector nor the gas system.

¹MONO-TORR PS4-MT15-R-2

²MKS mass flow controller

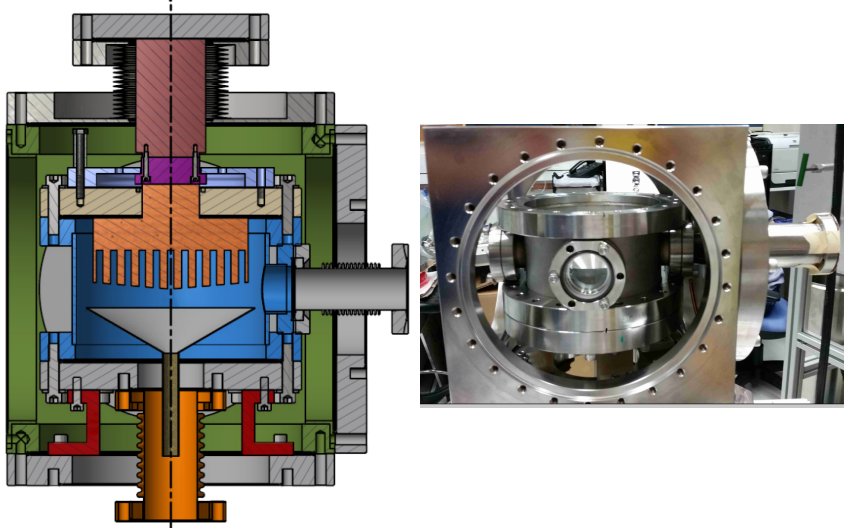


Figure 4. CAD view of the cryogenic system(Left) and a pictue of the cryogenic system (Right) .

87 The system is made out of two chambers, the outer vessel (OV) which holds the insulation
 88 vacuum, and the inner vessel (IV) that holds the xenon. In addition to the vacuum which prevents
 89 heat leaks from diffusion and convection, the entire IV is covered by multi layer aluminized Myler
 90 to prevent heating via radiation an image of the detector and the CAD design are shown in Fig 4.

91 The OV is made of a 10" CF cube, with ports on all six faces (e.g., FT, pumping ports, view
 92 ports). This vacuum is shared with the detector one via a 6" CF flexible bellows.

93 The IV is made of 1.5" height cylinder with 6" CF flanges on the top and bottom parts of it,
 94 and it holds inside xenon. A 120 mm diameter cold finger is welded to the top flange of the IV.
 95 The design of the cold finger is similar to the design of [13], the inner part of the cold finger is
 96 made of long fins, therefore the surface area of it is bigger resulting in a better heat transport. The
 97 upper part of the cold finger is in thermal contact with the cryo-cooler¹ via a cooper adapter. The
 98 copper adapter holds two 100Ω pt resistor which are connected to a PID reader² for temperature
 99 measurements. A Cartridge-heater is also inserted to the copper adapter for emergency heating.

100 The cryo-cooler provides up to 70 W of cooling power, and is connected via a 4½" flange to
 101 the OV top flange, and reaching the IV top flange. Common cryo-coolers used for xenon experi-
 102 ments, work in maximal cooling mode permanently. The QDrive, instead, has temperature control
 103 allowing it vary the cooling power, which enables to set the temperature with fluctuations smaller
 104 then 0.1 C° on the cooler itself.

105 On the inner side of the bottom flange of the IV a thin SS funnel is installed collecting all LXe
 106 drops from the cold finger, and delivering them to the detector part. This flange is connected to
 107 the detector part, via a 3½" flexible bellows. This bellows hosts two small pipes connected to the
 108 circulation system, and a third pipe coming from the funnel, all three pipes deliver LXe whereas the
 109 GXe is filling the bellows. The separation between the LXe coming from the gas handling system
 110 (clean) and the LXe coming from the cold finger (more dirty) allows the filling of clean LXe to

¹QDrive 20BB 9p6 A 3 AYNBNCO

²cryo-con model 18i Cryogenic Temp Monitor

111 different parts of the detector.

112 2.3 The Detector

113 [MMD: The detector refers to the chamber and its inner assembly that contains the liquid Xenon
114 bubble, the photomultiplier detectors around it and their accessories. This chamber is placed below
115 the cryogenic system. We describe the detector chamber and its interface to the cryogenic system
116 in section 2.3.1. In section 2.3.2 we discuss the assembly that consists of the HPFS sphere to hold
117 liquid Xenon and the Photomultiplier detectors distributed around the sphere.]

118 2.3.1 The Detector Chamber

119 The detector chamber is built such that apart from the interface to the cryogenic system, it can be
120 changed and modified easily for future experiments. The interface unit is built out of 2 flanges
121 welded together via 7 tubes, which serve as service ports for electrical and other feedthroughs. The
122 upper flange, ISO-K NW320, is part of the OV and shares the insulation vacuum of the cryogenic
123 system, the bottom one , CF-8", is part of an IV for future detectors, and would hold xenon inside.
124 For our experiment we modified the CF flange to fit also a $4\frac{5}{8}$ " CF flange which we use.

125 The OV is closed with a cylinder XXX cm height closed from the bottom with another ISO-K
126 NW320 flange, the height of the cylinder is determined such that the maximal height of the whole
127 apparatus is 190 cm, allowing the mobility of the detector through standard doors.

128 The $4\frac{5}{8}$ " CF flange is connected to a closed vessel internally divided into two parts. This vessel
129 serves as a xenon reservoir. The two parts of the vessel are connected to a spherical orb from above
130 (inner part) and from below (outer part). LXe is circulated such that new LXe drips into the outer
131 part and pumped from the inner one. This way the liquid level is controlled, and the sphere itself is
132 always filled with LXe.

133 2.3.2 The Sphere

134 The central component of the detector assembly is the hollow sphere which holds the LXe target
135 bubble. A spherical shell made of high purity fused silica with high transmittance is designed to
136 hold the LXe target. The xenon will be circulated Two invar tubes are connected to it from the top
137 and bottom with SS mini-CF flanges at the end, to circulate the xenon (see Fig.~[7](#)). The bottom
138 flange of the sphere is held using a brass holder to prevent force or torque applied on the sphere
139 while mounting the detector. The brass holder is connected to a plate held from the top 8" flange,
140 and is also used to align this plate at first installation. A set of 20 PMTs¹ are placed around the
141 sphere to detect light emitted from the LXe.

142 The LXe target bubble should not be too large in order to avoid double scatters. This shell
143 should be large enough to reduce internal reflections, but not too large which would attenuate the
144 scintillation light. The material of the shell should have a refractive index similar to LXe in order
145 to have minimal diffraction from the original direction of the photons when they travel from the
146 LXe target to the sphere. We chose corning HPFS 8655 as the shell material. The refractive index
147 of HPFS 8655 is 1.575 at 185 nm (LXe R.I. 1.61). In Fig. [5](#), are the refractive indices at various
148 wavelegths as given by the HPFS factsheet and also a naive extrapolation at lower wavelengths
149 which are relevant to us.

¹r8520-406 Hamamatsu 1" PMT

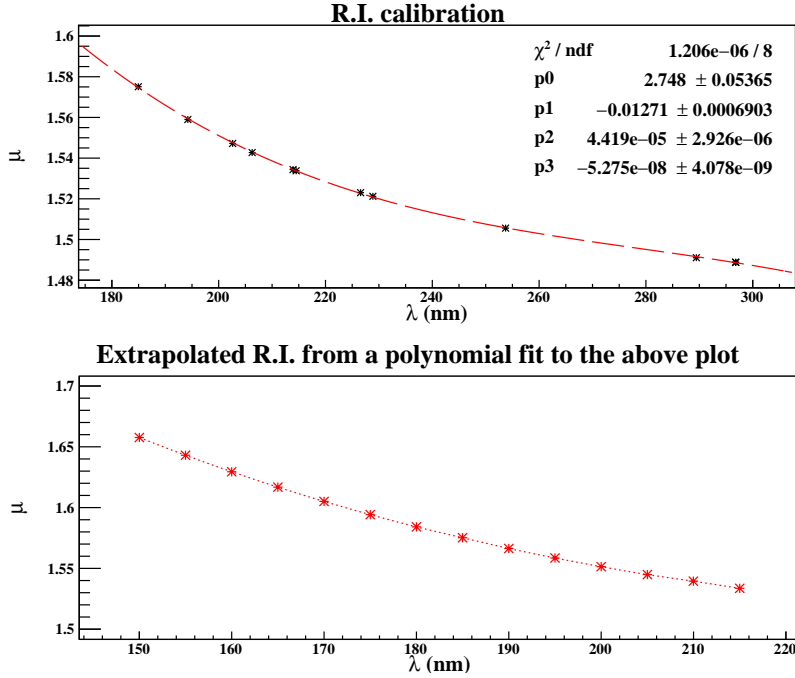


Figure 5. The refractive indices of HPFS 8655 at various wavelengths. (Top) The values provided from Corning factsheet. (Bottom) The values extrapolated at lower wavelengths.

150 The transmittance of the material is extremely crucial for us to optimize the dimension of the
 151 shell. Therefore, we obtained a 6 mm thick sample of HPFS 8655 and performed a transmittance
 152 testing a VUV monochromator setup. A deuterium light source was used to generate a spectrum
 153 in the range (110 - 950) nm, peaked approximately at 160 nm. The window of the light source
 154 faced a vacuum space pumped to below 10^{-4} Torr. The monochromator allows to select the desired
 155 wavelengths using a manually rotatable holographic diffraction grating. A PMT placed in the
 156 vacuum measured the intensity of light emitted from the monochromator, with and without the
 157 fused silica sample. The ratio of measured intensities was used to calculate the transmittance of
 158 the material. In fig. 6 is the measured transmittances/ 6 mm at (150 - 215) nm. At 175 nm the
 159 sample shows approximately 90%/6mm measured transmittance which corresponds to an intrinsic
 160 transmittance of about 98%.

161 The dimension of the fused silica shell is optimized by studying the path of the scintillation
 162 photons using a GEANT4 based simulation [14]. The sources that will be used for exciting the
 163 xenon, and creating the superradiance (signal) as well as the standard emission (background), will
 164 be ^{137}Cs (662 keV) and ^{57}Co (122keV & 136 keV) for ER and $^{241}\text{AmBe}$, D-D neutron generator,
 165 or neutron produced in an accelerator for NR . The mean free path for this energy is a couple of
 166 mm (^{57}Co) and (0.5 - 3) cm (^{137}Cs). We discuss the simulation in detail in section 4. The outer
 167 radius of the shell is 3 cm, while the inner radius of the hollow space that will hold the LXe is 1
 168 cm. The flow of the LXe will be maintained by two invar tubes. This shell–system, as is shown in
 169 Fig. 7 is being manufactured industrially as per the specification provided by us.

170 The photons coming out of the system will be detected by twenty 1" square Hamamatsu

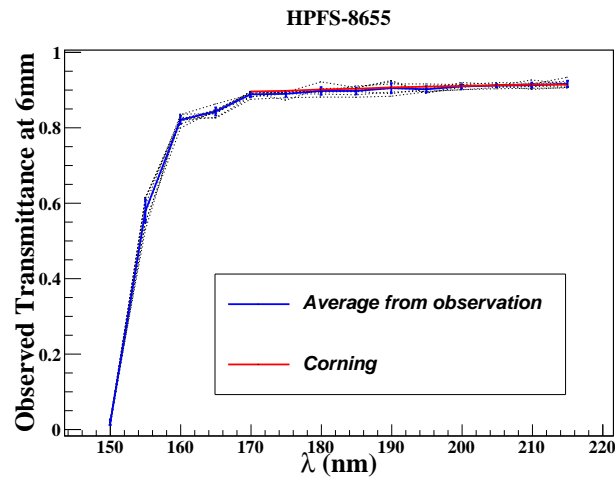


Figure 6. The transmittance of a 6 mm thick HPFS 8655 sample.

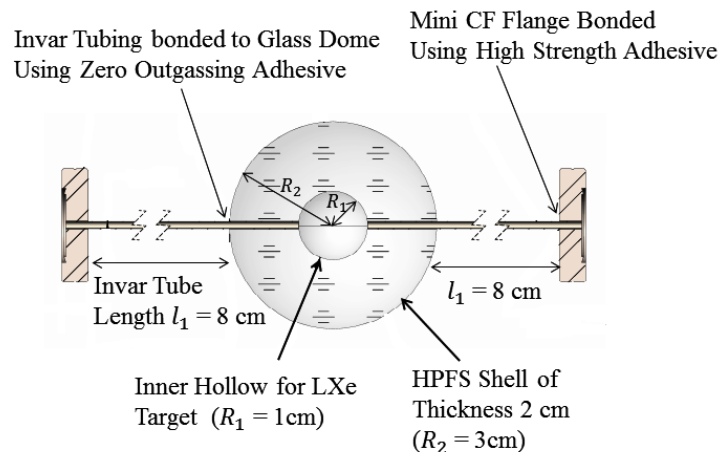


Figure 7. The technical scheme of the HPFS shell with invar tubing and flanges.

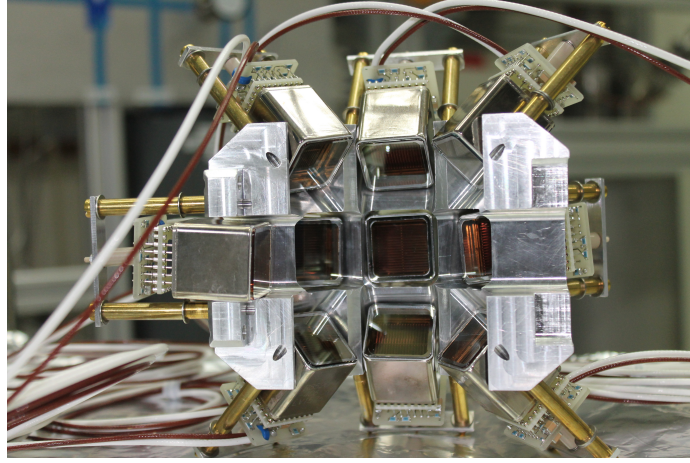


Figure 8. A PMT holder–hemisphere. We use two such components to hold 20 PMTS around the target.

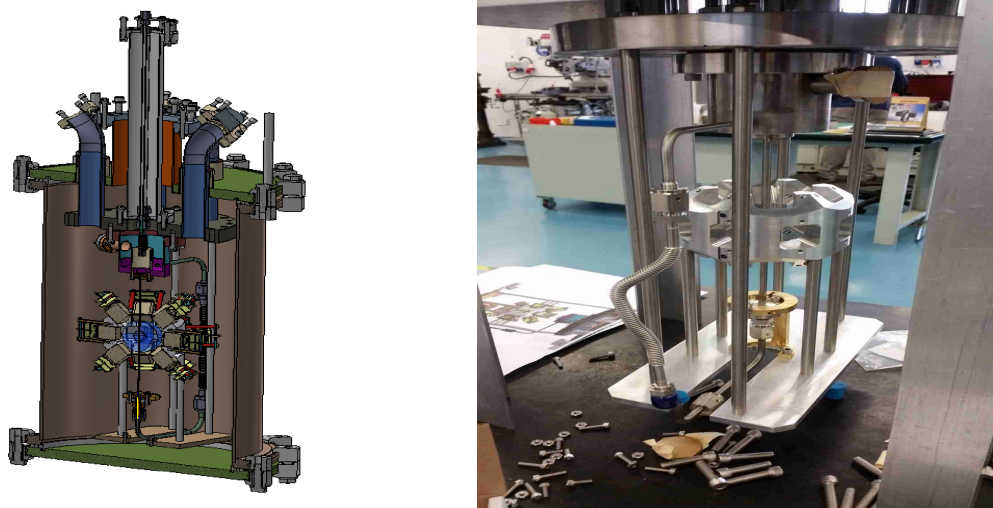


Figure 9. (Left) CAD design of the detector part. (Right) First mounting of the detector part, still not connected to the rest of the system.

R8520-406 photomultiplier tubes with an active area of $20.5 \text{ mm} \times 20.5 \text{ mm}$ each. We pick PMTs with a minimum quantum efficiency of 30% at 178 nm. For an applied voltage of 900 V the gain of these PMTs are 2×10^6 . We use a positive voltage divider, also manufactured by Hamamatsu, to provide high voltage to the PMTs. These 20 PMTs are held with a special aluminum holder, coated with anti-reflection substance. The holder is made of two hemispheres hosting the PMTs in 3 rows all of them pointing to the center of the fused-silica sphere. the PMTs are held only via their voltage–divider bases. The bases are held using M2 PEEK screws. In Fig. 8, one of the holder–hemispheres with the PMTs are shown.

In Fig. 9 we present a CAD schematic as well as a real view of the detector part.

180 **3 The Data Acquisition (DAQ) System**

181 [MMD: This part is almost complete, trigger logic details might get changed slightly]

182 In this section we discuss the data acquisition and readout from the PMT channels. We use a
183 heterogeneous system consisting of both NIM and VME electronics modules, with the data readout
184 being carried out through the VME controller module V2718 and a PCIe card A3818.

185 The schematic layout of the DAQ system is shown in Fig. 10. All the 20 PMTs are oriented
186 in the holder assembly which was discussed in section 2.3.2. The PMTs are ramped up to +800V
187 (the maximum is +900V) using a 24 channel VME high voltage distributor module ¹. We define
188 the raw electrical pulse output of the PMTs as S_i (raw), where $i = 1 - 20$. These raw pulses are
189 then amplified and shaped using two photomultiplier preamplifiers ². The preamplifier channels
190 operates from DC to 275 MHz and produce two identical $50\ \Omega$ non inverting outputs with voltage
191 gains of 10. We define the amplified pulses as S_i , ($i = 1 - 20$). One out of the two identical analog
192 outputs from each channel is converted to a digital signal with an Analog to Digitizer converter ³.

193 The ADC consists of two 12bit 5GS/s Switched capacitor Digitizer sections, each of them
194 with 16+1 channels, based on DRS4 chip. The dynamic range of the input signal is 1 Vpp with
195 adjustable DC offset. This module can sample either bipolar or unipolar analog input signal within
196 the dynamic range in a circular analog memory buffer, with default sampling frequency choices
197 5GS/s, 2.5 GS/s or 2 GS/s. As soon as a trigger signal reaches, all the analog memory buffers gets
198 frozen and then gets digitized into a digital memory buffer with a 12 bit resolution.

199 We generate an intrinsic trigger for the system, with the coincidence of any two out of the
200 twenty PMTs. The second output from the preamplifier channels are converted to binary signals
201 using two 16 channel leading Edge discriminator ⁴. In Fig. 10, we term the binary outputs from
202 the discriminator as SD_i , $i = 1 - 20$. The SD_i signals are then passed over to the logic module ⁵ to
203 obtain the trigger. At present, the coincidence of any two out of the twenty PMTs forms the trigger
204 logic. The output of the logic operation is used to trigger the ADC. In order to record the PMT
205 noise rate, the SD_i signals are duplicated and fed to a scaler ⁶.

206 The PMT event information and the trigger rate are read from the ADC, while the Scaler
207 records the PMT noise rate. The data readout to the acquisition PC is done through the Controller
208 and optical link to the master PCIe card. The further analyses of the relevant events in the PMTs
209 will be carried out offline using an analysis framework.

¹iseg VDS18130p

²Phillips 776. Each of the preamplifier model provides 16 independent and direct-coupled amplifiers channels

³CAEN ADC V1742: Switched capacitor Digitizer

⁴CAEN V895

⁵CAEN V1495, an FPGA based General purpose VME board which is programmed to perform the logic operation

⁶CAEN V830

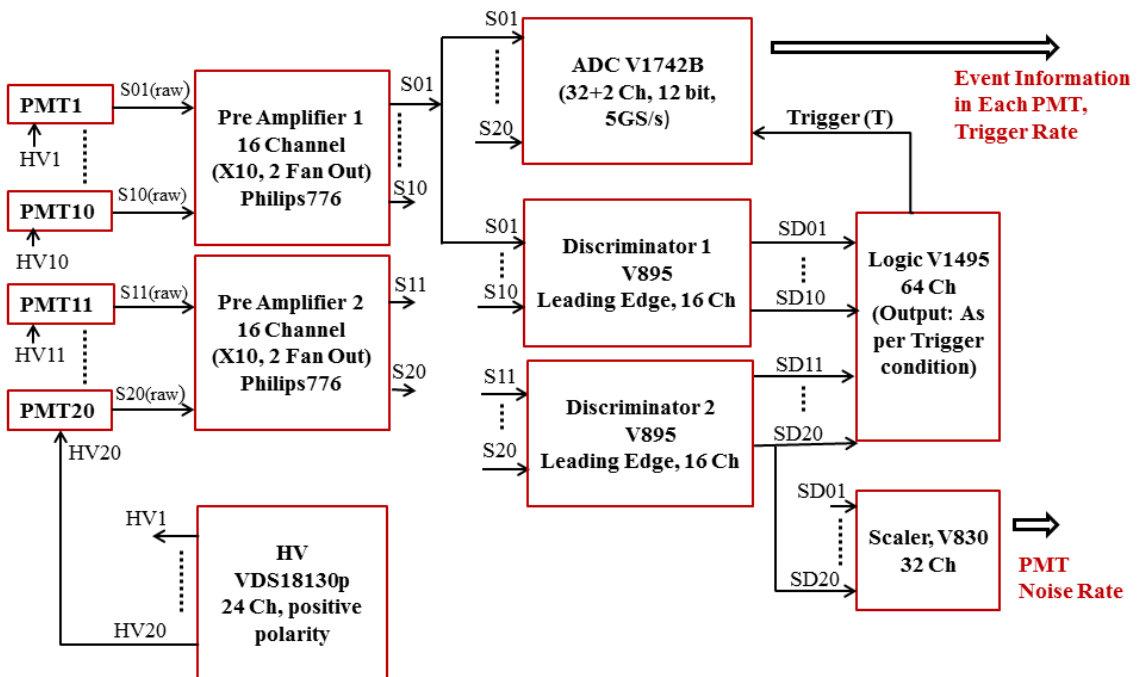


Figure 10. The schematic of the Data Acquisition System of Direxeno. It consists of 20 PMTs and the subsequent electronic channels to record the events for an internal trigger generated by the coincidence of any two PMTs in the system and also the PMT noise rate.

210 **4 Simulation**

211 In this section we present the Monte Carlo simulation study that was performed to optimize the
212 geometry and performance of the LXe scintillation detection system. We perform a GEANT4 based
213 simulation to obtain the reasonable dimensions of the spherical LXe holder and the placement of the
214 PMT detectors around it, which is described in section 4.1. In section 4.2, we discuss the statistical
215 test performed to find the detector’s sensitivity in measuring various patterns of the scintillation
216 emission from the LXe target.

217 **4.1 The Detector Geometry**

218 We perform a study to optimize the dimensions of the setup using a GEANT4 based framework
219 that includes realistic description of the target, the enclosing HPFS sphere and the PMTs around.
220 The simulations takes into account the physics processes of the propagation of the photons from
221 the LXe target through the the sphere and the vacuum and their interaction at the PMTs. The
222 parameters under test for this study are the size of the sphere, the PMT size and their placement
223 around the sphere. The refractive index and internal transmittance of both of LXe and of HPFS are
224 known with good precision.

225 For the simulation, we fix all parameters except the outer radius (R_2) of the sphere. The fixed
226 parameter values are chosen by quantitative physical considerations and educated guesses. The
227 radius of the LXe target R_1 will determine the event rate for a particular source, and we choose
228 it to be 1 cm. The conventional PMTs designed by Hamamatsu to detect scintillation from LXe
229 are 1" and 3" square PMTs, and we choose the 1' ones in order to get better spatial resolution. an
230 array of 20 PMTs around the sphere, placed at a distance of 39 mm from the centre of the targetare
231 considered. The active area of each PMT is 22 mm \times 22 mm.

232 In order to chose a reasonable dimension of the sphere, we first study the detection efficiency
233 of scintillated photons in the simulated setup. Using an inotropic emmision of 50photons/event,
234 we find the average ratio of the detected photons/event to the net emitted photons/event, for various
235 choices of R_2 . The trasmittance of HPFS is a crucial parameter and we vary it within a large range
236 to check the impact of it. The photon detection ratio for different sets of R_2 and transmittance are
237 shown in Fig. ??.

238 **4.2 The statistical test**

239 **5 Summary**

240 **References**

- 241 [1] E. Aprile and T. Doke. Liquid Xenon Detectors for Particle Physics and Astrophysics. *Rev. Mod.*
242 *Phys.*, 82:2053–2097, 2010.
- 243 [2] A. Rubbia. Future liquid Argon detectors. 2013. [*Nucl. Phys. Proc. Suppl.* 235-236, 190(2013)].
- 244 [3] J. Silk et al. *Particle Dark Matter: Observations, Models and Searches*. Cambridge Univ. Press,
245 Cambridge, 2010.
- 246 [4] E. Aprile et al. First Dark Matter Search Results from the XENON1T Experiment. 2017.

- 247 [5] D. S. Akerib et al. Results from a search for dark matter in the complete LUX exposure. *Phys. Rev. Lett.*, 118(2):021303, 2017.
- 248
- 249 [6] Changbo Fu et al. Spin-Dependent Weakly-Interacting-Massive-ParticleâŠNucleon Cross Section
250 Limits from First Data of PandaX-II Experiment. *Phys. Rev. Lett.*, 118(7):071301, 2017.
- 251
- 252 [7] J. Aalbers et al. DARWIN: towards the ultimate dark matter detector. *JCAP*, 1611:017, 2016.
- 253
- 254 [8] R. H. Dicke. Coherence in spontaneous radiation processes. *Phys. Rev.*, 93:99–110, Jan 1954.
- 255
- 256 [9] M. Gross and S. Haroche. Superradiance: An essay on the theory of collective spontaneous emission.
Physics Reports, 93(5):301 – 396, 1982.
- 257
- 258 [10] N G Basov, V A Danilychev, and Yurii M Popov. Stimulated emission in the vacuum ultraviolet
region. *Soviet Journal of Quantum Electronics*, 1(1):18, 1971.
- 259
- 260 [11] Frederick H. Mies. Stimulated emission and population inversion in diatomic bound-continuum
transitions. *Molecular Physics*, 26(5):1233–1246, 1973.
- 261
- 262 [12] K L Giboni, X Ji, H Lin, A Tan, T Ye, Y Zhang, and L Zhao. A liquid xenon development and test
system. *Journal of Instrumentation*, 9(04):T04006, 2014.
- [13] E. Aprile et al. The XENON100 Dark Matter Experiment. *Astropart. Phys.*, 35:573–590, 2012.
- [14] S. Agostinelli et al. GEANT4: A Simulation toolkit. *Nucl. Instrum. Meth.*, A506:250–303, 2003.